CALCULATION AND COMPARATIVE ANALYSIS OF IR SPECTRA OF A NUMBER OF BRASSINOLIDES WITH DIFFERENT SIDE-CHAIN STRUCTURES

V. M. Andrianov and M. V. Korolevich[*]   UDC 547.455:535.33/34:539.194

Experimental IR spectra and theoretical spectral absorption curves of the practically important biologically active steroid phytohormones (22S,23S)-24-epibrassinolide, (22S,23S)-28-homobrassinolide, and homobrassinolide, which have similar chemical structures, were compared and analyzed to establish spectral and structural correlations of them. This enabled an evaluation of the influence of side-chain structural features on the formation of IR spectra and the establishment of connections between their structural differences and the observed changes in the IR spectra in the range 1500–950 cm^{-1}.

Introduction. Brassinolides and castasterones are biologically active hormones of the phytohormonal steroid (PS) class. They help to improve the quality of plant products, are toxic to rapidly spreading tumor cells, and are considered potential anticancer pharmacological agents [1–4]. This group of steroids numbers greater than 70 compounds [5–7]. The biological activity of these compounds is known to depend substantially on the stereochemical configuration of the C22 and C23 atoms and the structure and configuration of the side-chain C24 alkyl substituent [8]. These could be important to the toxicity of brassinolide and castasterone derivatives for a whole series of cancer cells [9, 10].

IR spectroscopy offers huge possibilities for obtaining information about molecular structures. However, recorded IR spectra of series of PSs have been analyzed only in a few studies [11–13]. Theoretical investigations are needed to establish structure–spectra correlations in practically important biologically active PSs. These include modeling of the molecular structure, calculation of vibrational spectra, and comparative analysis of experimental and calculated IR spectra of structurally similar molecules of this compound class. Previously, vibrational spectra were fully calculated and optical-density spectral curves were modeled by us for the biologically active PSs (22S,23S)-24-epicastasterone [14], 24-epicastasterone [15], homobrassinolide, and (22S,23S)-24-epibrassinolide [16].

The aim of the present work was to compare and analyze IR spectra of natural homobrassinolide and synthetic (22S,23S)-24-epibrassinolide and (22S,23S)28-homobrassinolide, which have similar chemical structures, to evaluate the influence of structural differences in the side chains of these molecules on the formation of their IR spectra using total calculation of the frequencies and intensities of normal modes and to model the optical-density spectral curves of them in the crystalline state.

Experimental. The starting geometric parameters of (22S,23S)-28-homobrassinolide and (22S,23S)-24-epibrassinolide were taken from x-ray structure analyses [17, 18]; of homobrassinolide, from molecular modeling of its crystal structure. An original combined approach to the analysis of IR spectra of complicated organic compounds that was developed and programmed for studying spectra of carbohydrates was used to calculate the frequencies and intensities of normal modes. It combined a classical analysis of normal modes with quantum-chemical evaluation of absolute intensities corresponding to integrated intensities of IR absorption bands. The algorithm for calculating intensities has been described in detail [19].

---

[*]To whom correspondence should be addressed.

Belarusian State Agrarian Technical University, Minsk, Belarus; email: korolevi@dragon.bas-net.by. Translated from Zhurnal Prikladnoi Spektroskopii, Vol. 88, No. 4, pp. 513–524, July–August, 2021. Original article submitted April 13, 2021.

Frequencies, shapes, potential-energy distributions (PEDs) of normal modes, and atomic shifts in Cartesian coordinates in each normal mode for calculating absolute intensities of IR absorption bands were calculated using a molecular mechanics (MM) method. The force field developed by us for calculating the frequencies and shapes of normal modes by the MM method for brassinosteroids was published [14]. Optical-density spectral curves corresponding to crystalline synthetic (22S,23S)-24-epibrassinolide, (22S,23S)-28-homobrassinolide, and natural homobrassinolide were modeled based on the results.

Results and Discussion. (22S,23S)-24-Epibrassinolide (I) consists of 82 atoms; (22S,23S)-28-homobrassinolide (II) and homobrassinolide (III), 85 atoms that form two six-membered (A and C), one seven-membered (B), and one five-membered ring (D) and a bulky side chain. The structural differences of these molecules are localized within the side chains, which have different configurations of the 22- and 23-diol groups (22S,23S in I and II and 22R,23R in III) and different substituents in (methyl in I and ethyl in II and III) and configurations of the 24-position (24R in I and 24S in II and III). For convenience of recognizing the differences in the configurations of neighboring side-chain C atoms in the 22,-, 23-, and 24-positions, we will use the designations SSR (I), SSS (II), and RRS (III).

(22S,23S)-24-Epibrassinolide

(22S,23S)-28-Homobrassinolide

Homobrassinolide
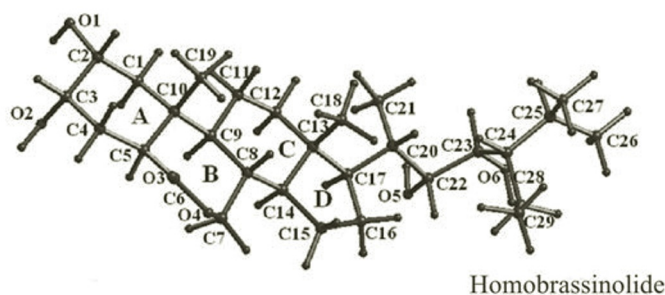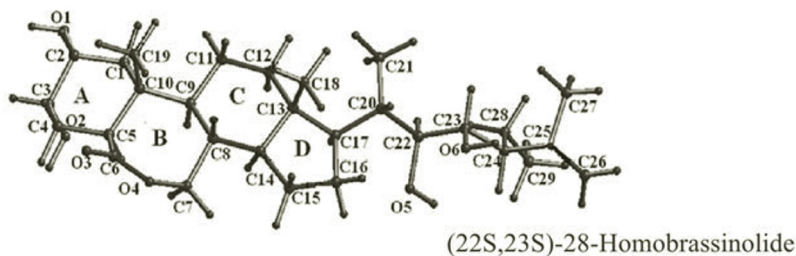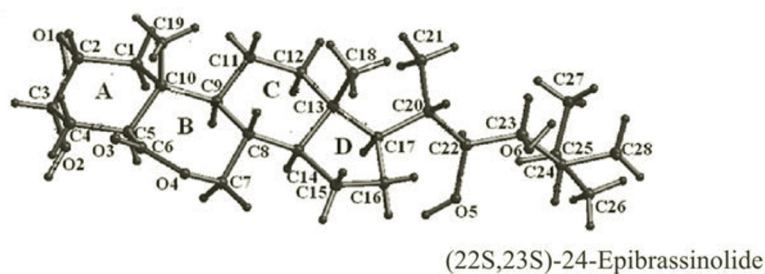
IR spectra of I and III were previously analyzed by comparing experimental and theoretical absorption spectra [16]. Structurally similar II was also included in the analysis in the present work to establish more reliable structure–spectra correlations. The analyzed IR spectra were recorded on a NEXUS FTIR spectrometer. Samples of the compounds were ground with dried finely disperse KBr. The resulting powders were compressed under vacuum by the standard method. Theoretical spectra were calculated using quasi-isolated molecules. The effect of intermolecular interactions, in particular intermolecular H-bonds, on the vibrational spectra were not considered. Most attention was paid to the range 1500–950 cm^{-1}, which is often used for analytical purposes.

Many of the numerous normal modes are weak in the IR spectra. However, Fig. 1 shows that the density of vibrational states in this range is rather large. Theoretical spectra are presented as an envelope of Gaussian bands (Fig. 1a–c) and as vertical lines (Fig. 1d–f) showing the positions and intensities of the calculated normal modes. Figure 2 shows the calculated and experimental absorption spectra. Table 1 lists the assignments of the absorption bands of the studied molecules in the analyzed spectral range. A comparison of the theoretical and experimental spectra showed that
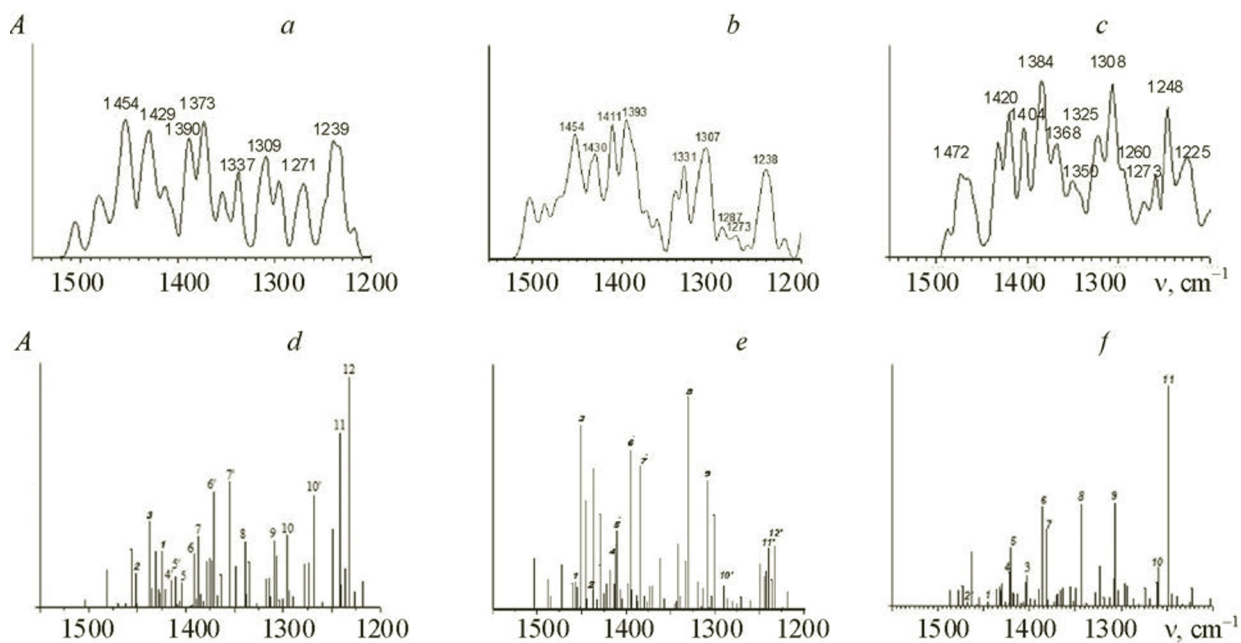
Fig. 1. Theoretical IR absorption spectra as Gaussian band envelopes (a–c) and as vertical lines (d–f) of (22S,23S)-24-epibrassinolide (a, d), (22S,23S)-28-homobrassinolide (b, e), and homobrassinolide (c, f) in the range 1500–1200 cm^{-1}; numbers denote normal modes.

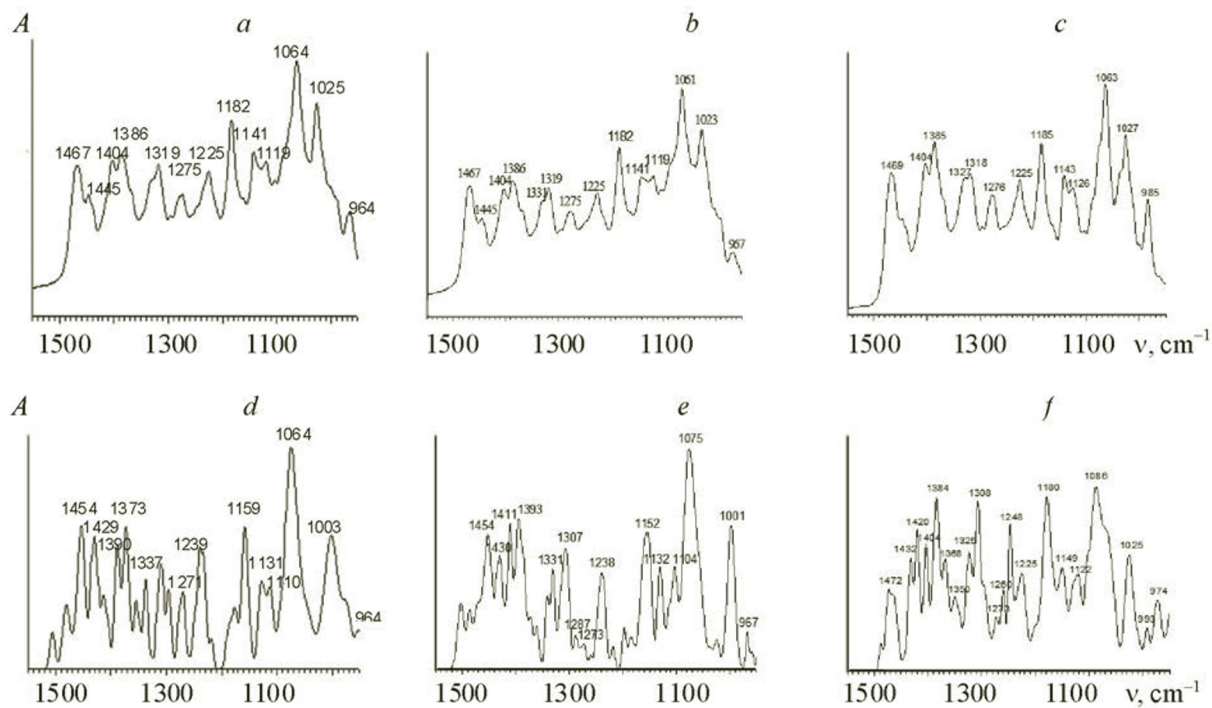Fig. 2. Experimental (a–c) and theoretical IR absorption spectra (d–f) of (22S,23S)-24-epibrassinolide (a, d), (22S,23S)-28-homobrassinolide (b, e), and homobrassinolide (c, f) in the range 1500–1200 cm^{-1}.

TABLE 1. Experimental (IR) (ν_{exp}) and Calculated (ν_{calc}) Frequencies (cm^{-1}), Absolute Intensities A (10^{16} cm^2·mol^{-1}·s^{-1}), and PED of Normal Modes of Crystalline (22S,23S)–24-Epibrassinolide (I) [16], (22S,23S)–28-homobrassinolide (II), and Homobrassinolide (III) [16] in the Range 1500–950 cm^{-1}

$\nu_{exp}(\nu_p)$	ν_{calc} I	ν_{calc} II	ν_{calc} III	A I	A II	A III	PED, % I	PED, % II	PED, % III
1467	1507	1503	1487	6	30	6	HC21H 34 CC21H 17 CC23H 7 CC12H 7	HC21H 33 CC21H 17	CC11H 29 HC1H 12 CC1H 12 CC18H 7 HC18H 7
(1454)	1481	1488	1477	24	17	6	CC11H 14 HC11H 13 CC1H 12 HC1H 11 HC18H 9 CC18H 9	CC11H 15 CC1H 15 HC11H 12 HC1H 11	HC19H 34 CC19H 31 HC4H 6 CC4H 5
1467	1470	1472	1473	2	26	8	HC18H 25 CC18H 23 HC1H 6 CC1H 5 CC11H 5 HC12H 5	HC18H 28 CC18H 25 HC1H 5 CC1H 5	HC18H 21 CC18H 18 HC21H 11 CC21H 10 HC1H 5
(1454) 1467	1462	1460	1472	2	15	2	HC12H 21 CC12H 19 HC18H 9 CC18H 8 HC11H 5	HC12H 22 CC12H 20 CC18H 7 HC18H 7 HC11H 6 CC11H 5	HC28H 28 C24C28H 22 CC22H 7 CC24H 6 CC29H 5
(1472)	1456	1457	1463	38	16	21	HC7H 26 C8C7H 15 O4C7H 7 HC4H 6 CC8H 6	HC27H 42 C25C27H 39	HC4H 28 CC4H 25 HC19H 12 CC19H 7
	1451	1455	1457	21	13	1	HC28H 32 CC28H 30 CC27H 9 HC27H 9	HC19H 20 CC19H 18 HC4H 11 CC4H 10 HC1H 7	HC12H 16 CC12H 14 HC21H 11 CC21H 10 HC18H 7 CC18H 6 HC11H 5
	1450	1451	1455	2	110	3	HC4H 32 CC4H 27 HC7H 7 CCC 5	HC19H 18 CC19H 17 HC4H 12 CC4H 10 HC11H 5	HC1H 13 CC1H 11 HC11H 11 CC11H 9 HC12H 7 HC18H 7 CC12H 6
1445 (1429)	1437	1445	1445	56	65	1	CO5H 13 CC23H 10 CC22H 9 CCC + CCO 9 (s.c.) OCH 8 (s.c.)	HC7H 25 O4C7H 11 C8C7H 11 CC8H 8 HC18H 7	HC27H 41 C25C27H 38
1445 (1430)	1435	1437	1436	12	11	6	CO2H 17 CC4H 9 CC3H 9 CC1H 9 O2C3H 7 HC1H 6 CC3O2 5	HC29H 26 CC29H 24 HC26H 15 CC28H 10	HC18H 21 HC19H 10 HC7H 8 O4C7H 6 CC8H 5
1445 (1432)	1431	1436	1436	33	84	3	HC18H 18 HC26H 15 CC28H 14	CO2H 19 CC4H 10 CC3H 8 CC1H 9 O2C3H 7 HC1H 6 CC3O2 5	CO2H 12 HC18H 11 CC3H 7 CC1H 6 CC4H 6 HC19H 6 O2C3H 5
	1428	1429	1432	11	57	7	CO6H 13 CCC 8 (s.c.) CC23H 7 HC28H 7 O6CH 6 CC28H 6	CO6H 15 CCC 11 (s.c.) CC24H 8 O6CH 7 HC26H 7 CC29H 6	HC19H 15 HC18H 10 HC15H 10 CC15H 10 HC7H 7 O4C7H 5
	1428	1429	1431	3	26	6	HC15H 12 CC15H 12 CC1H 8	HC15H 17 CC15H 17 HC18H 13	HC19H 24 HC15H 8 CC15H 8 HC7H 6 O4C7H 5
	1427	1425	1430	9	9	9	CC1H 12 CC1H 9 HC15H 7 CC15H 7 HC1H 5	CO1H 15 CC1H 8 CC21H 6	HC18H 16 HC15H 10 CC15H 10 HC7H 10 O4C7H 8 HC19H 6
	–	–	1426	–	–	2			CC24H 8 CC20H 7 CC22H 6 C23O5H 5 HC21H 6 HC26H 6 HC29H 5 CC29H 5

700

TABLE 1. (Continued)

ν_exp(ν_p)	ν_calc			A			PED, %		
	I	II	III	I	II	III	I	II	III
1404 (1390)	1424	1422	1422	36	15	13	HC27H 26 CC27H 24 CC28H 10 HC28H 11 CC25H 6	HC21H 18 CC1H 16 CC1H 9 HC18H 8	HC26H 13 HC29H 11 CC29H 10 HC27H 7 HC21H 7 CC27H 6
1404 (1411)	1421	1418	1420	11	23	23	HC21H 19 CC21H 17 HC18H 10 CC1H 8	HC19H 34 CC11H 10 CC19H 6 CC1H 6 HC21H 6 CC21H 5	HC27H 15 CC27H 13 HC21H 8 CC21H 6 C23O5H 5
1404 (1420	1415	1413	1418	8	15	5	HC28H 13 HC26H 10 CC28H 6 CC1H 7 CC11H 7 COH 5	HC26H 36 CC26H 21 CC28H 6 HC29H 10 CC29H 9	HC29H 12 HC27H 11 CC29H 11 CC27H 10 HC26H 9
	1415	1412	1417	17	33	5	CC11H 10 CC1H 9 HC28H 9 HC26H 6 COH 5	HC19H 23 CC11H 11 CC19H 5 C2O1H 5 CC1H 5	CC1H 17 C2O1H 6 CC2H 6 CC11H 5 HC1H 5 HC19H 5 CCO 5
	1411	1412	1413	19	18	5	HC16H 29 CC16H 26 CCC 6	HC16H 27 CC16H 25 HC19H 6 CCC 6 (s.c.)	CC20H 10 CC24H 10 CC23H 6 C23O5H 5 C22O4H 5 HC21H 5
	1406	1410	1409	4	47	1	HC18H 41 CC18H 11	HC19H 18 CC11H 13 HC18H 8 CC12H 6	HC19H 32 CC11H 11 CC19H 7
	1404	1406	1404	15	11	9	HC27H 56 HC28H 12 CC27H 12	HC18H 31 CC11H 9 C13O18H 8 C20CC21H 5 HC21H 5	HC16H 23 CC16H 21 CC14H 6 HC18H 6
	1395	1398	1404 1402	1	15	8 12	HC19H 30 CC11H 8 CC19H 8 CC12H 7	CO5H 17 CC23H 9 CC20H 6 CO6H 5	HC18H 16 CC11H 14 CC12H 6 HC11H 5 CO5H 14 CC24H 9 CO6H 8 CC20H 6 HC27H 5 CC22H 5 CCC 5
1386 (1373)	1393	1395	1394	2	95	1	HC27H 39 CC25H 9 HC26H 9 CC27H 7	HC29H 32 HC26H 19 C24C28H 5 C25C26H 5 C28C29H 5	CC14H 28 CCC 5 HC15H 5 CC15H 5 HC16H 5
1386	1391	1394	1394	34	11	2	CC14H 24 HC19H 6 CC17H 5	CC14H 26 HC15H 5 CCC 5 C14C15H 5 CC17H 5	HC29H 53 HC27H 12 CC29H 11
1386 (1393)	1387	1388	1389	46	3	7	CC1H 18 C2O1H 11 HC19H 7 CC11H 6 CC14H 5	CC1H 18 C2O1H 13 CC11H 6	HC29H 56 CC29H 9 HC27H 9 CC28H 8
1385	1385	1388	1386	8	8	39	HC28H 46 HC26H 16 CC28H 11	HC29H 19 CC22H 8 CC28H 8 HC27H 7 CC29H 7 CC23H 7	CC1H 25 C2O1H 14 CC11H 7 HC1H 5 C3O2H 5 CC2H 5
(1385)	1382	1387	1381	3	5	31	HC19H 41 CC19H 13 CC1H 7 CO1H 5	HC27H 40 C25C27H 11 HC29H 11	HC26H 61 C25C26H 16
	1378	1384	1380	29	85	2	HC21H 10 CC23H 8 CC25H 6 CC22H 5 HC27H 5	HC29H 20 CC23H 11 CC22H 9 HC21H 5 C23O6H 5	HC21H 42 CC21H 10
	1375	1379	1373	31	8	2	CC4H 25 CC1H 8 CC3H 6 CC5H 5	CC4H 25 CC1H 8 CC3H 7 CC5H 5 HC21H 5	CC17H 9 CC22H 8 C25C24H 7 COH 5 (s.c.)
	1373	1376	1371	30	4	4	HC21H 11 (O4C7H + CC7H) 6 CC25H 6 CC9H 5	HC21H 12 CC9H 9 CC7H 8 CC4H 7	CC4H 16 CC5H 13 CC9H 6
	1371	1373	1369	75	13	5	HC21H 13 O4C7H 8 CC7H 8 CC17H 7 CC8H 6	HC21H 20 CC9H 8 CC7H 6 CC8H 6 O4C7H 5	CC24H 10 O5CH 6 CO5H 5 CO6H 5 O6CH 5 CC23H 5 CC25H 5 CC20H 5
	1368	1370	1366	7	14	6	CC17H 16 O4C7H 6 CC7H 6 CC14H 5	CC17H 20 CC14H 5 CC16H 5	CC17H 12 CC22H 6 CC24H 5 CC20H 5 CC25H 5
	1364	1362	1363	21	30	7	CC9H 15 CC12H 8 CC17H 6 HC21H 5	CC9H 11 C8C7H 8 C7C8H 8 O4C7H 7 CC12H 6	CC7H 11 CC9H 9 CC4H 7 CC8H 7 HC7H 5
	1355	1357	1355	81	6	7	CC23H 12 CC24H 10 CC22H 9 CC25H 6 COH 7 (s.c.)	CC23H 14 CC28H 14 CC22H 5 CC25H 5 CC24H 5	CC22H 12 CC28H 8 CC25H 6 CC17H 6 C22O4H 5 CC24H 5

TABLE 1. (Continued)

$\nu_{exp}(\nu_p)$	ν_{calc} I	ν_{calc} II	ν_{calc} III	A I	A II	A III	PED, % I	PED, % II	PED, % III
1331	1348	1345	1349	26	3	7	CC25H 15 CC23H 10 CC24H 7 O6C23H 5 COH 6 (s.c.)	CC25H 7 CC28H 7 CC20H 6 CC22H 6 OC7H 5 CCC 5	C7C8H 11 C8C7H 8 O4C7H 7
(1337)	1339	1341	1343	42	39	42	CC5H 7 CC12H 7 CC2H 7 CC3H 5 CC9H 5	CC5H 9 CC12H 8 CC3H 6 CC2H 5 O1C2H 5	CC8H 9 CC9H 8 CC12H 8 CC2H 5
1331	1335	1333	1338	30	28	1	CC24H 10 CC25H 7 CC9H 5 CC20H 5	CC25H 14 C29C28H 8 C24C28H 6 CC12H 5	CC28H2 14 CC20H 10 CC23H 8 CC22H 7 CC24H 5
(1331)	1327	1330	1323	2	127	16	CC12H 13 CC11H 8 CC9H 6 CC14H 5	CC12H 13 CC11H 7 CC9H 5 CC28H 5	CC4H 7 CC12H 6 CC5H 6 C1C2H 5 O1C2H 5
1327 (1325)	1317	1319	1319	18	16	3	CC5H 8 CC16H 7 CC20H 7	CC5H 9 CC16H 5 CC20H 5	CC20H 7 CC25H 6 CC22H 5
1319 (1309)	1314	1313	1313	18	12	3	CC12H 8 CC5H 7 CC15H 7 CC9H 7 CC11H 6 CC16H 5	CC15H 7 CC16H 6 CC22H 6 CC14H 5 CC5H 5 CC12H 5 CC20H 5	CC8H 7 CC14H 6 CC28H 6 CC7H 6 CC23H 5 CC25H 5
1319 (1307)	1309	1308	1308	43	77	11	CC2H 13 C2C3H 10 CC5H 9 O1C2H 6 CO2H 5 O2C3H 5	CC2H 11 CC5H 6 CC12H 6 CO2H 5 C2C3H 5 O2C3H 5 O1C2H 5	CC28H 10 O5C22H 6 CC23H 6 CC25H 6CC20H 5 CC24H 5 CC8H 5
1318 (1308)	1307	1306	1307	33	1	41	CC9H 9 CC8H 9 CC15H 8 CC16H 8 CC22H 7	CC9H 13 CC8H 6 CC12H 6 CC15H 5	CC2H 16 CC4H 11 CC5H 6 C2C3H 6 O2CH 5 CO2H 5 CC1H 5
	1304	1304	1303	4	7	6	CC16H 12 CC15H 11 CC20H 9 CC22H 5	CC16H 15 CC20H 13 CC15H 12 CC9H 5	CC16H 17 CC15H 14 CC8H 7 CC12H 6
	1300	1301	1296	5	56	9	CC16H 7 CC22H 7 CC24H 7CC8H 6 CC14H 5 CC17H 5 CC20H 5	CC16H 8 CC14H 8 CC8H 6 CC20H 6 CC22H 6 CC17H 5 CC23H	CC5H 10 CC16H 6 CC17H 5
1275 (1271)	1296	1290	1293	47	14	8	CC5H 14 CC4H1 10 CC2H 7	CC5H 20 CC4H1 10 CC1H 8 CC9H 6 CCC 6 CC2H 5 O1C2H 5	CCH 11 (s.c.) CCH (skelet) 10 CC5H 9 CC9H 5
1275 (1273)	1294	1286	1286	11	6	3	CC24H 8 CC25H 8 CC20H 7 CC23H 5	CC24H 9 CC20H 8 CC23H 5 CC8H 5 CC22H 5	CC9H 11 CC20H 6 CC24H 6 CCH 6 (skel.) CCH 6 (s.c.) CC11H 5
1276 (1273)	1278	1280	1274	27	5	7	CC1H 11 CC8H 7 CC5H 5 CC16H 5	CC1H 13 CC5H 7	CC25H 12 CCH 9 (skelet.) CC23H 8 CC24H 7 CC15H 6 O5CH 5
	1273	1271	1269	28	7	3	CC8H 6 CC1H 6 CC25H 5 CC24H 5	CC8H 10 CC20H 7 CC24H 7 CC25H 5 CC16H 5	CC1H 15 CC5H 8 O1C2H 7 CC3H 6 CC4H 6 CO2H 5
	1268	1260	1261	72	5	9	OCH 8 (s.c.) CC25H 7 CC20H 6 CC24H 5 CC8H 5	CC15H 13 CC16H 8 CCC 8 CC17H 7 CC8H 7 CC1H 7 CC20H 6	CCH 12 (s.c.) CC15H 11 CC16H 8 CC12H 6 CC17H 5 CC25H 5 CCC 5
			1259			15			CC24H 10 CC25H 10 O6C23H 6 CC23H 5 O5C22H 5 CC17H 5

TABLE 1. (Continued)

ν_exp(ν_p)	ν_calc			A			PED, %		
	I	II	III	I	II	III	I	II	III
1225 (1239)	1249	1249	1248	51	26	87	CC2H 8 CC11H 8 CC20H 6 CC14H 6 CC12H 5	CC2H 7 CC11H 7 CC14H 6 CC12H 5 CC17H 5 CC20H 5	O4C7H 7 CC 6 CCC 5 CC4H 5 CC9H 5 C5C6=O3 5 O4C6=O3 5 CC7H 5
	1241	1242	1245	113	23	5	CC1H 7 CC2H 6 CC17H 5 CC8H 5	CC1H 7 CC2H 7 CC17H 5	CC11H 6 CC12H 6 CC20H 6 CC14H 6 C17H 5
1225 (1238)	1240	1239	1239	14	37	4	CC17H 10 CC11H 10 CC15H 7 CC5H 5 CC12H 5 O4C7H 5	CC17H 10 CC11H 8 CC15H 8 CC24H 8 CC5H 6 CC12H 5	CC1H 9 CC2H 9 CC3H 6 CC17H 6
1225 (1225)	1236	1236	1233	24	17	1	CC23H 8 CC20H 8 CC24H 7 O6CH 7 CO6H 6 O5CH 6 CCC 5	CC23H 10 CC20H 9 CCC 7 CO6H 6 O5CH 6 CC22H 5 O6CH 5	CC11H 10 CC17H 10 CC15H 9 CC12H 8 CC16H 6 CC11H 5
		1233	1225	150	38	2	CC17H 6 CC11H 6 CC12H 6 CC1H 6 CC5H 5 CC15H 5	CC17H 7 CC5H 6 CC11H 6 CC12H 6 CC1H 5 CC15H 5	CC3H 18 CC4H 7 CC11H 7 C3O2H 6 C1C2H 6 O1C2H 5
	1226	1224	1223	9	1	7	CC11H 16 CC15H 10 CC16H 8 CC8H 6	CC11H 18 CC15H 9 CC16H 7	CC11H 18 CC15H 8 CC16H 7
	1218	1218		17	10	–	CC3H 23 CC4H 12 C1C2H 7 O1C2H 7 C3O2H 6	CC3H 24 CC4H 13 C1C2H 7 O1C2H 7 C3O2H 6 CCO 6 CC1H 5	–
1182 (1159)	1188	1198	1202	3	28	3	CC17H 7 CC18H 6 CCC 6 CC4H 6 CC1H 5 CC12H 5	C24C28H 14 C29C28H 11 CC24H 7 CC25H 7 CCC 6 CC 6	C24C28H 11 C29C28H 9 CC25H 9 CCC 7 (s.c.) CC22H 7 CC24H 6
1182 (1152)	1187	1185	1183	3	8	4	CC1H 11 CC4H 10 CC11H 5 CC5H 5 CC19H 5	CC4H 15 CCC 7 CC3H 6 CC5H 6 OC3H 5 CC2H 5 CC1H 5	CC7H 7 CC19H 6 CC2H 5 CC5H 5 CC15H 5 CC11H 5
1185 (1180)	1176	1180	1181	9	6	10	CC24H 6 CC25H 6 CCC 5	CC4H 8 CCC 6 C10C19H 5 CC15H 5	CC1H 20 CC4H 9 O4C7H 8 C10C19H 7 CCC 7 CC2H 5
	1162	1161	1174	28	7	11	CCH 13 (skelet.) CCH 13 + OCH 5 (s.c.)	O4C7H 6 CC12H 5 CCC 5	CCC 8 O4C7H 6 C10C19H 5 CC5H 5
	1156	1155	1159	14	5	5	CC12H 9 O4C7H 7 CC7H 8 CCC 5 CC15H 5	CC12H 8 O4C7H 7 CC7H 7 CCC 5 CC18H 5	CCH 14(skelet.)CC7H 7 CC22H 6 CCH 6 (s.c.)
	1156	1151	1150	22	15	3	CC16H 6 CC7H 6 CC14H 6 CC11H 5 CC18H 5 CCC 5	CC11H 6 CC12H 5 CC15H 5 CC16H 5	CCH 17(skelet.)O4C7H 6 C8C7H 6 CC15H 5
1141 (1131)	1149	1147	1149	14	15	3	CC15H 9 CC8H 6 CC7H 5 CC17H 6 CC16H 5 CCC 5	CC8H 8 CC7H 8 CC12H 6 CC11H 5 CC15H 5 CC17H 5	CC11H 7 CC17H 6 CC18H 5 CC14H 5 CCC 5 CC15H 5 CC22H 5
1141 (1132)	1131	1133	1137	16	27	1	CC2H 9 CC3H 8 CC4H 8 CC 7 CCC 7 CCO 6 OC2H 6 COH 5	CC28H 24 CC27H 7 CC22H 6 CC23H 5 CC25H 5 CC29H 5	CC28H 20 CCH 17(s.c.) O5CH 5
1143 (1149)	1129	1131	1131	8	15	15	CC16H 20 CC12H 8	CC3H 9 CC2H 9 CC4H 7 CCC 7 OC2H 6 CCO 6 O2C3H 5	CCC 11 CCH 10(skelet.)CC3H 8 OC2H 6 CC1H 6 CC2H 5 C2OH 5 CC12H 5
	1124	1125	1124	15	18	6	CC12H 7 CC + CO 6 CC16H 5 CC2H 5 O1C2H 5	CC12H 8 CC16H 7 CC 7 CC2H 6 O1C2H 5	CCH 15(skelet.) CC16H 13 O4C7H 5 CC21H 5 CC28H 5

TABLE 1. (Continued)

ν_exp(ν_p)	ν_calc			A			PED, %		
	I	II	III	I	II	III	I	II	III
1119 (1112)	1118	1114	1119	12	31	13	CC16H 9 CC 7 (s.c.) CC26H 6 CC25H 5 CC20H 5 O5CH 5	CC4H 13 CC3H 5	CC12H 10 CC2H 9 CC3H 7 CCO 7 CC4H 6 CC 6 O2C3H 5
1119	1112	1113	1114	9	2	4	delocalized	CC16H 10 CC4H 6 CC22H 5 O5C22H 5	CC16H 13 O4C7H 11 C8C7H 9 CC12H 7 CC15H 6
(1104)	1111	1104	1105	25	86	23	CC4H 12 CC16H 9 CC3H 5	CC16H 7 CC4H 6 CC3H 5 CC15H 5	CC4H 17 CC16H 7 CCC 7
1126 (1122)	1104	1100	1092	6	7	10	CC4H 10 CC16H 7 CC12H 6 CC15H 5 CC3H 5	CC28H 14 CCC 13 (s.c.) CC29H 8 CC25H 6 CC24H 5	CC12H 15 CC4H 12 CC16H 5
1064 (1074)	1082	1081	1088	8	67	8	(O4C7H + CC7H) 7 CC16H 7 OCH 7 (s.c.) CC15H 6 CCC 5	(O4C7H + CC7H) 12 CC25H 7 CC26H 5 CC16H 5 CC12H 5	CCH 14 (s.c.) CC16H 12 CCH 8 (skel.) CCC 5
1061 (1075)	1079	1081	1080	17	1	4	O4C7H 6 CC7H 5 OCH 6 (s.c.) CC16H 5	(O4C7H + CC7H) 10 CC25H 9 CC26H 7 CC16H 6	CCH 20 (s.c.) CC15H 8 CCH 6 (skel.) (CCO+CCC) 6 (s.c.)
	1073	1074	1069	6	10	11	CC15H 8 O4C7H 6 CC2H 6 O2C3H 5 CC16H 5	CC15H 7 CC2H 6 OC7H 6 CCC 6 CC 5 O2C3H 5 CC16H 5	CCH 16 (skelet.) CCC 11 O2C3H 6 CC2H 6 CC4H 6 CCO 5 CC 5
1063 (1086)	1072	1073	1063	13	8	2	CC16H 12 CC15H 7 O4C7H 6	OC22H 7 OC23H 6 OC7H 6 CC21H 5 CC 5 + CCO 5 + CCC 6 (s.c.)	(CCH 18 CCC 13) (s.c.) CC15H 7 CC 5 CC21H 5
	1068	1070	1058	4	6	2	CC26H 9 CC27H 8 CCC 7 (s.c.) CC15H 5 CC16H 5	CC16H 15 CC15H 8	O5CH 5 CC27H 5
	1063	1062	1056	4	19	1	CC15H 22 CC16H 5	CC15H 22 CC16H 7	CC16H 25 CC15H 15 CCH 7 (skelet.)
	1056	1055	1051	3	3	3	CC15H 8 CCC 8 O4C7H 7 CC19H 5	CC15H 12 CC27H 6 CC26H 6 O4C7H 5 CC12H 5	CC15H 16 CCH 9 (skelet.) CCH 7(s.c.) CC16H 5
	1045	1054	1047	1	1	1	CC21H 11 CCC 8 (s.c.) CC18H 6	C25C26H 8 C25C27H 8 CCC 6	CC15H 16 CCH 11 (skelet.) CCC 9 CC14H 5 CC12H
	1042	1044	–	3	1	–	CCC 17 CC15H 10 CC18H 8 CC 6 CC16H 6 CC8H 5	CC21H 10 CCC 10 (s.c.) CC18H 5 CC27H 5 CC26H 5	CC26H 15 CC27H 12 (CCH 13 CCC 7 CC 6) (s.c.) C24C28H 5 / –
1025 (1003)	1023	1035	1030	2	4	2	CCC 9 CC11H 8 CC19H 8 O4C7H 6 CC12H 6	CCC 15 CC15H 10 CC18H 8 CC16H 6 CC 6 CC8H 5	CCC 16 CCH 10 (skelet.) O4C7H 8 CC15H 7 CC16H 5 CC8H 5 CC18H 5
1023 (1001)	1009	1024	1025	8	8	5	CCC 13 CC15H 8 CC 6 CC17H 5	CCC 10 CC11H 8 CC19H 7 O4C7H 5 CC12H 5	CCH 17 (skelet.) CCH1 11 (s.c.) CCC 5
1027 (1026)	1009	1009	1010	1	1	2	CC27H 14 CC26H 12 CC28H 12 CC21H 8 CCC 5 (s.c.)	CCC 17 CC15H 10 CC 7 CC17H 5	CC29H 15 CC21H 8 CC26H 8 CCC 8 (s.c.) CC28H 6
999	999	998	1004	16	56	1	CC19H 15 CCC 11 CC3H 8 CC 5 CCO 5	CC29H 25 C24C28H 18 CC27H 6 CC26H 6 CC21H 6	CCC 12 CC15H 10 CCH 9 (skelet.) CC16H 5 CC29H 5 CC 5
992	992	995	994	4	14	2	CC28H 16 CC21H 13 CCC 9 (s.c.) CC27H 6 CC26H 6	CC19H 13 CCC 15 CC3H 8 CC 6	C28C29H 16 CC21H 13 C24C28H 7 C29C28H 6
975	975	–	–	12	–	–	CC28H 21 CC27H 13 CC26H 11 CCC 7 (s.c.) CC21H 6	–	–

TABLE 1. (Continued)

$\nu_{exp}(\nu_p)$	ν_{calc}			A			PED, %		
	I	II	III	I	II	III	I	II	III
964 (954)	954	967	992	7	43	3	CC19H 21 CCC 9 CC7H 8 HC19H 6 CC18H 5	CC18H 12 CC21H 10 CC29H 7 CC15H 6 CC16H 5 CCC 5	CC19H 13 CCC 11 CC3H 7 CC 5 CC4H 5
967	946	958	973	9	10	8	CC18H 14 CC15H 12 CC16H 9 CC21H 9	CC18H 20 CC21H 19	CC29H 14 CC21H 12 CCC 9 CC18H 7
(967) 985	935	945	958	1	37	1	CC19H 17 CC11H 8 CC21H 6 HC19H 5	CC18H 11 CC15H 9 CC21H 7 CC16H 5 CC27H 5 CC19H 5	CC18H 20 CC21H 14 CC15H 6 CC16H 5 CC29H 5
(974)	–	941	951	–	62	4	–	CC19H 18 CC4H 6 CC27H 5	CC19H 22 C8C7H 5 CC11H 5 CC21H 5
			950	–	–	1	–	–	CCH 12 (skelet.) CC19H 11 CC18H 7 CC15H 6
									CC4H 6 CC11H 5 CCC 5
			945	–	–	3	–	–	CC15H 10 CC18H 9 CC21H 8 CC19H 7 CC16H 6

Note. s.c., side chain; frequencies ν_p of absorption band maxima of theoretical spectra of I, II, and III are given in parentheses.

705

the theoretical spectra were in general satisfactorily described by the main and strongest characteristic absorption bands of the examined region. For example, the maximum frequency shift of corresponding ν_{calc} and ν_{exp} bands was from 14 cm^{-1} (1500–1200 cm^{-1} range) to 23 cm^{-1} (1200–950 cm^{-1}) for I, from 13 to 30 cm^{-1} for II, and from 10 to 23 cm^{-1} for III.

Table 1 lists the calculated frequencies, PEDs, and absolute intensities of normal modes located in the studied region that contributed most to the intensity of the summed band and the frequencies of band maxima in the theoretical spectra. It can be seen that each band of the experimental spectra had a complicated origin and consisted of several bands of various integrated intensities (the sum of Gaussian bands over the calculated absolute intensities and half-widths set from 8 to 16 cm^{-1}). For example, the strong band with two maxima at 1467 (I and II), 1469 (III), and 1445 cm^{-1} in the experimental spectra (1500–1425 cm^{-1}) consisted of 15 (I and III) and 18 (II) constituent components.

The high-frequency part of this band with maxima at 1469 (III) and 1467 cm^{-1} (I and II) in the studied compounds was formed mostly by bending vibrations of methyl and methylene groups. The low-frequency part with a maximum at 1445 cm^{-1} originated in bending vibrations involving methyl and methylene groups and hydroxyls. An analysis of the data in Table 1 also suggested that slight structural differences in the molecules shifted the frequencies of several normal modes of similar shapes. In particular, conformational differences in the terminal part of their side chains affected the frequencies and intensities of normal vibrations with the main contribution to the PED of methyl and methylenes located in just this part of the side chain. For example, the normal mode with the main contribution to the PED from bending of C27H$_3$ methyl bonds had a frequency of 1424 cm^{-1} in I, 1457 cm^{-1} in II, and 1445 cm^{-1} in III.

Replacing the C28H$_3$ methyl (**I**) in the side-chain C24-position by a C28H$_2$C29H$_3$ ethyl (II and III) led to the appearance (instead of the normal mode with the main contribution to the PED from bending of C28H$_3$ methyl bonds with a frequency of 1451 cm^{-1}) of a normal mode with the main contribution to the PED from bending of groups in the C28H$_2$C29H$_3$ ethyl in II at 1437 cm^{-1} and in III at 1472 cm^{-1}. Figure 1 shows lines corresponding to these normal modes that are designated 1 and 2. The high-frequency shift [1398 (II), 1402 (III), 1437 cm^{-1} (I)] (Fig. 1, line 3) of the normal mode for the O5H hydroxyl and C22H and C23H methyls of the side-chain diol group could be explained by the configuration change of the C24–C28 bond [24S (II and III) and 24R (I)].

A change of the intensity ratio of the spectral maxima was characteristic of the second strong band in the range 1500–1200 cm^{-1} with two maxima at 1404, 1385 (III), and 1386 cm^{-1} (I and II) in the experimental spectra (1425–1350 cm^{-1}) of the studied molecules. Also, the ratio of the peak intensity changed as compared to peak intensities of close-lying bands in the experimental spectra. This band strengthened with respect to bands with maxima at 1467 (I and II) and 1469 (III) and 1319 (I and II) and 1318 cm^{-1} (III) on going from I and II to III. The ratio of peak intensities in these molecules followed an analogous trend in the theoretical spectra (Fig. 2).

An analysis of Table 1 showed that bending vibrations of methyls C26H$_3$, C27H$_3$, and C29H$_3$ situated in the terminal part of the side chain in III (1422 and 1420 cm^{-1}, Fig. 1, lines 4 and 5) contributed most to the intensity of the high-frequency portion of the band with a maximum at 1404 cm^{-1}; in II, bending vibrations of methyl C19H$_3$ located at the junction of rings *A* and *B* of the molecular skeleton (1412 and 1410 cm^{-1}, lines 4′ and 5′). Highly active bending vibrations of methyl C27H$_3$ (1424 and 1404 cm^{-1}, lines 1 and 5) and bending vibrations of methylenes C16H$_2$, C11H$_2$, and C1H$_2$ of the molecular skeleton (1415 and 1411 cm^{-1}, lines 4′ and 5′) in I contributed noticeably to the high-frequency portion of this band. Normal modes with vibrational energy localized on both atoms incorporated into the molecular skeleton (ring *A*, 1386 cm^{-1}, line 6) and in the terminal part of the side chain (1381 cm^{-1}, line 7) contributed most to the calculated integrated intensity of the low-frequency portion of this band with a maximum at 1385 cm^{-1} in III. Conversely, normal modes with the main contribution to the PED of HCH and CCH bending vibrations of ethyl C28H$_2$C29H$_3$ that was immediately adjacent to the diol group (1395 and 1384 cm^{-1}, lines 6′ and 7′) had the greatest absolute intensity in the calculated spectrum of II. Normal modes with the main contribution to the PED of HCH and CCH bending vibrations in the calculated spectrum of I both in the molecular skeleton (1391 and 1387 cm^{-1}, lines 6 and 7) and in the diol group and the atomic group immediately adjacent to it (1371 and 1355 cm^{-1}, lines 6′ and 7′) had the greatest absolute intensities. Because the diol located on C22 and C23 had different configurations in I and II (22S,23S) and III (22R,23R), it obviously had different effects on the frequencies and intensities of the normal modes in this range. Thus, the main changes in the ratios of both the maximum intensities at 1404 and 1385 (III) and 1386 cm^{-1} (I and II) and its intensity and close-lying bands in experimental spectra of the studied molecules were related to the different configurations of the diol and conformations of the side-chain terminal part as this band formed in them.

A third strong band of the experimental spectra in the range 1500–1200 cm^{-1} was located in the range 1350–1300 cm^{-1}; had maxima at 1319 (I and II) and 1318 cm^{-1} (III) [at 1309 (I), 1307 (II), and 1308 cm^{-1} (III) in the

calculated spectra] and shoulders at ~1331 (I and II) and 1327 cm^{-1} (III) [1337 (I), 1331 (II), and 1325 cm^{-1} (III)] (Fig. 2); and consisted according to the calculations of 12 (I) and 13 (II and III) components. Delocalized CCH bending vibrations (and OCH to a lesser extent) of all methine (CH) and methylene (CH$_2$) groups of the molecular skeleton made the main contribution to the formation of this band. These vibrations [1339 and 1309 cm^{-1} (I), 1330 and 1308 cm^{-1} (II), 1343 and 1307 cm^{-1} (III)] (Fig. 1, lines 8 and 9) in rings *A* and *C* of the molecular skeleton contributed most to the intensity (Table 1). Two weaker bands in this range with maxima at 1275 (I and II) and 1276 cm^{-1} (III) [1271 (I), 1273 (II), and 1273 and 1260 cm^{-1} (III) in the calculated spectra] and 1225 cm^{-1} [1239 (I), 1238 (II), and 1225 cm^{-1} (III)] (ranges 1300–1250 and 1250–1200 cm^{-1}) (Fig. 2) consisted according to the calculation of six (I and II) and seven (III) and eight (I and II) and seven band components (III), respectively. Like for the band discussed above, delocalized CCH bending vibrations of methines and methylenes made the main contribution to their formation (Table 1). A change in the intensity ratio of their peak intensities in experimental spectra of the studied molecules, i.e., a decrease in the intensity of the first band on going from III to I and II, was a characteristic feature of these two bands. An analogous trend was observed in the calculated spectra of these molecules (Fig. 2). Table 1 also shows that normal modes in which the vibrational energy was localized on diol groups and neighboring side-chain groups (1259 cm^{-1}, Fig. 1, line 10) contributed most to the integrated intensity of the first band in the calculated spectrum of III; vibrations involving the molecular skeleton [1296 cm^{-1} (I), line 10 and 1290 cm^{-1} (II), line 10′] and the diol and neighboring side-chain groups [1268 cm^{-1} (I), line 10′], in I and II.

Delocalized CCH bending vibrations of methine (CH) and methylene groups (CH$_2$) of the molecular skeleton, among which normal modes with frequencies 1248 (III), 1239 and 1233 (II) (Fig. 1, lines 11, 11′, and 12′), and 1241 and 1232 cm^{-1} (**I**) (lines 11 and 12) contributed most to the integrated intensity despite the structural differences of these molecules being localized in the side chains, made the main contribution to the formation of the band at 1250–1200 cm^{-1} in these molecules. It could be assumed that the change in the intensity ratio of the absorption bands in this range was related to the different configurations of the side-chain diol.

Experimental spectra of the studied compounds in the range 1200–900 cm^{-1} consisted of a strong band with maxima at 1182 (I and II) and 1185 cm^{-1} (III); a doublet with maxima at 1141 (I and II) and 1143 (III) and 1119 (I and II) and 1126 cm^{-1} (III); and a broad absorption band with two clearly resolved maxima at 1064 (I), 1061 (II), and 1063 (III) and 1025 (I), 1023 (II) and 1027 cm^{-1} (III) (Fig. 2). The strong band with maxima at 1185 (III) and 1182 cm^{-1} (I and II) in the experimental spectrum (1200–1150 cm^{-1}) consisted according to the calculations for the studied compounds of 11 components, the main contribution to the formation of which came from bending vibrations of CCH and OCH methines and methylenes, CCC bending vibrations in the skeleton and side chain, and C–C stretching vibrations. This band strengthened relative to the absorption band with a maximum at ~1225 cm^{-1} on going from III to I and II.

Distinguishing features of this band as compared to those discussed above were a shape change of the vibrations in most normal modes forming it and a more noticeable role of the side chain, in particular, ethyl C28H$_2$C29H$_3$. The absolute intensity of the normal mode at 1198 cm^{-1} in II increased significantly as compared to the analogous vibration at 1202 cm^{-1} in III. Bending vibrations of atomic moieties located in rings *A* and *B* in III and in rings *B*, *C*, and *D* in I made the main contribution to its formation. These were normal modes with frequencies 1181 and 1174 (III) and 1162 and 1156 cm^{-1} (I). It could be assumed that these changes in the formation of this band were associated with the different diol configurations of side-chain C22 and C23 of I, II, and III and with the different configurations of the C24–C28 bond [R (I) and S (II and III)].

Also, ethyl C28H$_2$C29H$_3$ in II played an important role in the calculations in forming a doublet with maxima at ~1141 (I and II) and 1143 (III) and 1119 (I and II) and 1126 cm^{-1} (III) in the experimental IR spectra (1150–1100 cm^{-1}). Bands with maxima at 1131 and 1112 (I), 1132 and 1104 (II), and 1149 and 1122 cm^{-1} (III) in the theoretical spectra corresponded to them (Fig. 2). Bending vibrations of ethyl CC28H contributed greatly in addition to CCH and OCH bending vibrations of methines and methylenes of the molecular skeleton to the total intensity of this doublet in II. This affected the intensity ratio of both maxima in this doublet absorption band (Fig. 2).

Experimental spectra of the molecules in the range 1100–950 cm^{-1} showed a broad absorption band with two maxima that were strongest in the range 1500–950 cm^{-1} at 1064 (I), 1061 (II), and 1063 (III) and 1025 (I), 1023 (II), and 1027 cm^{-1} (III) and a weaker band at ~985 (III) and a shoulder at ~964 (I) and 967 cm^{-1} (II) (Fig. 2). According to the calculations, these bands consisted of 20 component bands. An analysis of Table 1 showed that CCH bending vibrations of methyls, CCH and OCH bending vibrations of methines and methylenes, and bending (CCC) and stretching vibrations (C–C) of the skeleton and side chain made the main contribution to the formation of these strong maxima [at 1074 (I), 1075 (II), and 1086 (III) and 1003 (I), 1001 (II), and 1025 cm^{-1} (III) in the theoretical spectra].

The activities of the $C15H_2$ and $C16H_2$ methylenes in five-membered ring *D* and the $C7H_2$ methylene in seven-membered ring *B* were noteworthy. The CCH and OCH bending vibrations involving these groups contributed noticeably to the integrated intensity of experimental bands with maxima near 1064 (I), 1061 (II), and 1063 (III) and 1025 (I), 1023 (II), and 1027 cm^{-1} (III). Furthermore, the ethyl (methyl in I) on side-chain C24 (and the C24–C28 configuration) had a significant effect on the formation of bands at 1025 (I), 1023 (II), and 1027 cm^{-1} (III) in experimental spectra of the studied molecules. For example, the normal mode in II at 998 cm^{-1} that made the main contribution to the PED of the bending vibration of the CCH localized in this group had the maximum absolute intensity as compared to normal modes of this frequency range and contributed most to the integrated intensity of the band maximum at 1001 cm^{-1} in the theoretical spectrum, which corresponded to the band maximum at 1023 cm^{-1} in the experimental spectrum. Normal modes close to it in III (1010 and 994 cm^{-1}) with noticeable contributions to the PED of the ethyl CCH bending vibrations contributed less to the integrated intensity of the analogous band (1027 cm^{-1}). As a result, the intensities of band maxima at ~1027 (III) and 1023 cm^{-1} *(II) changed on going from III to II i*n the theoretical and experimental spectra of the studied molecules.

Bending vibrations of CCH groups localized in this group and those adjacent to it in **I** made the main contribution to the PED of normal modes with frequencies 1009, 992, and 975 cm^{-1} and contributed noticeably to the integrated intensity of the band maximum at 1003 cm^{-1} in the theoretical spectrum, which corresponded to the band with a maximum at 1025 cm^{-1} in the experimental spectrum. A weaker band at ~985 cm^{-1} in the low-frequency region of this spectral range of III transformed into a shoulder at ~967 cm^{-1} in the spectrum of II and at ~964 cm^{-1} in that of I (Fig. 2).

According to Table 1, the normal mode (973 cm^{-1}) with a significant contribution to the PED of the bending vibration of the CC29H methyl in the side-chain ethyl contributed noticeably to the integrated intensity of this band in the experimental spectrum of III. However, normal modes of atomic moieties in the molecular skeleton contributed noticeably to the integrated intensity in this range for I and II. Therefore, it could be proposed that the intensity change (transformation into a shoulder) of this absorption band in spectra of I and II was related to the different configurations of the side-chain diol.

Conclusions. A comparative analysis of calculated vibrational spectra of structurally similar PSs allowed a relationship to be found between their structural differences and changes of the IR spectra. It was found that small differences in the molecular structures led to either shape changes of several normal modes with similar frequencies or frequency shifts of several normal modes with similar shapes. As a result, the integrated intensities, shapes, and half-widths of the corresponding absorption bands changed. It was also found that differences in the C22 and C23 diol configuration (22S,23S in I and II and 22R,23R in III) and the conformation of the terminal part of the side chain in the studied molecules had large effects on the integrated intensities, shapes, and half-widths of absorption bands with maxima near 1404 and 1385 (III), 1386 (I and II), 1276 (III), 1275 cm^{-1} (I and II) and 1225, 1143 (III), 1141 (I and II) and 1126 (III), 1119 (I and II) and 1027 (III), 1025 (I), 1023 (II), and 985 cm^{-1} in the experimental IR spectra.

REFERENCES

1. Y. Zhou, C. Garcia-Prieto, D. A. Carney, R. Xu, H. Pelicano, Y. Kang, W. Yu, C. Lou, S. Kondo, J. Liu, D. M. Harris, Z. Estrov, M. J. Keating, Z. Jin, and P. Huang, *J. Natl. Cancer Inst.*, **97**, 1781–1785 (2005).
2. T. Nakata, T. Yamada, S. Taji, H. Ohishi, S. Wada, H. Tokuda, K. Sakuma, and R. Tanaka, *Bioorg. Med. Chem.*, **15**, 257–264 (2007).
3. E. Hovenkamp, I. Demonty, J. Plat, D. Lutjohann, R. P. Mensink, and E. A. Trautwein. *Prog. Lipid Res.*, **47**, 37–49 (2008).
4. T.-M. Wang, T. Hojo, F.-X. Ran, R.-F. Wang, R.-Q. Wang, H.-B. Chen, J. R. Cui, M. Y. Shang, and S. Q. Cai, *J. Nat. Prod.*, **70**, 1429–1433 (2007).
5. V. A. Khripach, V. N. Zhabinskii, and A. E. de Groot, *Brassinosteroids: A New Class of Plant Hormones*, Academic Press, San Diego, CA (1999).
6. J. L. Nemhauser and J. Chory, *J. Exp. Bot.*, **55**, 265–270 (2004).
7. Y. Hu, F. Bao, and J. Li, *Plant J.*, **24**, 693–701 (2000).
8. S. Drosihn, A. Porzel, and W. Brandt, *J. Mol. Model.*, **7**, 34–42 (2001).
9. J. Malikova, J. Swaczynova, Z. Kolar, and M. Strnad, *Phytochemistry*, **69**, 418–426 (2008).
10. A. Yu. Misharin, A. R. Mehtiev, V. N. Zhabinskii, V. A. Khripach, V. P. Timofeev, and Ya. V. Tkachev, *Steroids*, **75**, 287–294 (2010).
11. N. A. Borisevich, I. V. Skornyakov, V. A. Khripach, G. B. Tolstorozhev, and V. N. Zhabinskii, *J. Appl. Spectrosc.*, **74**, 673–680 (2007).

12. N. A. Borisevich, D. K. Buslov, V. N. Zhabinskii, and V. A. Khripach, *J. Appl. Spectrosc.*, **76**, 617–622 (2009).

13. N. A. Borisevich and D. K. Buslov, *J. Appl. Spectrosc.*, **77**, 491–495 (2010).

14. V. M. Andrianov and M. V. Korolevich, *J. Appl. Spectrosc.*, **75**, 771–778 (2008).

15. V. M. Andrianov and M. V. Korolevich, in: *Proceedings of the International Scientific Conference "Molecular, Membrane, and Cellular Principles of Biosystem Functioning"* [in Russian], June 23–25, 2010, Minsk (2010), Vol. 1, pp. 302–304 (2010).

16. V. M. Andrianov, M. V. Korolevich, and A. A. Velchenko, *J. Appl. Spectrosc.*, **86**, No. 6, 965–974 (2019).

17. L. Kutschabsky, G. Adam, and H.-M. Vorbrodt, *Z. Chem.*, **30**, 136–145 (1990).

18. L. Kutschabsky and G. Reck, Private Communication to the Cambridge Structural Database, deposition number CCDC 201799 (2003).

19. M. V. Korolevich, *Analytical Infrared Spectroscopy of Saccharides*, Doctoral Dissertation in Physical-Mathematical Sciences, Minsk (2009).